Electronic Supplementary Material (ESI) for Inorganic Chemistry Frontiers.

MOFs containing linear bis-pyridyl tris-amide and angular carboxylates: exploration of proton conductivity, water vapor and dye sorptions

Satyanarayana K Konavarapu, Anindita Goswami, Anaparthi Ganesh Kumar, Susanta Banerjee [b] and Kumar Biradha*[a]

CCDC numbers: MOFs 1-4: 1856603-1856606

Table of contents

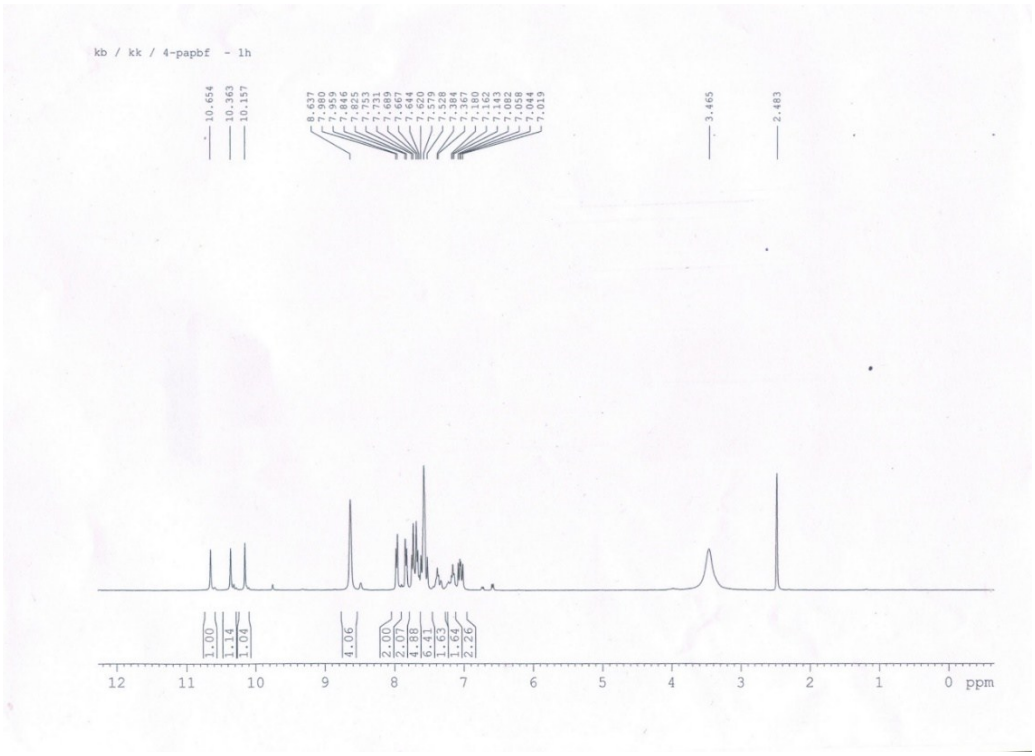

Figure S1: ^{1}H NMR (400 MHz in D6DMSO) for the ligand **L**

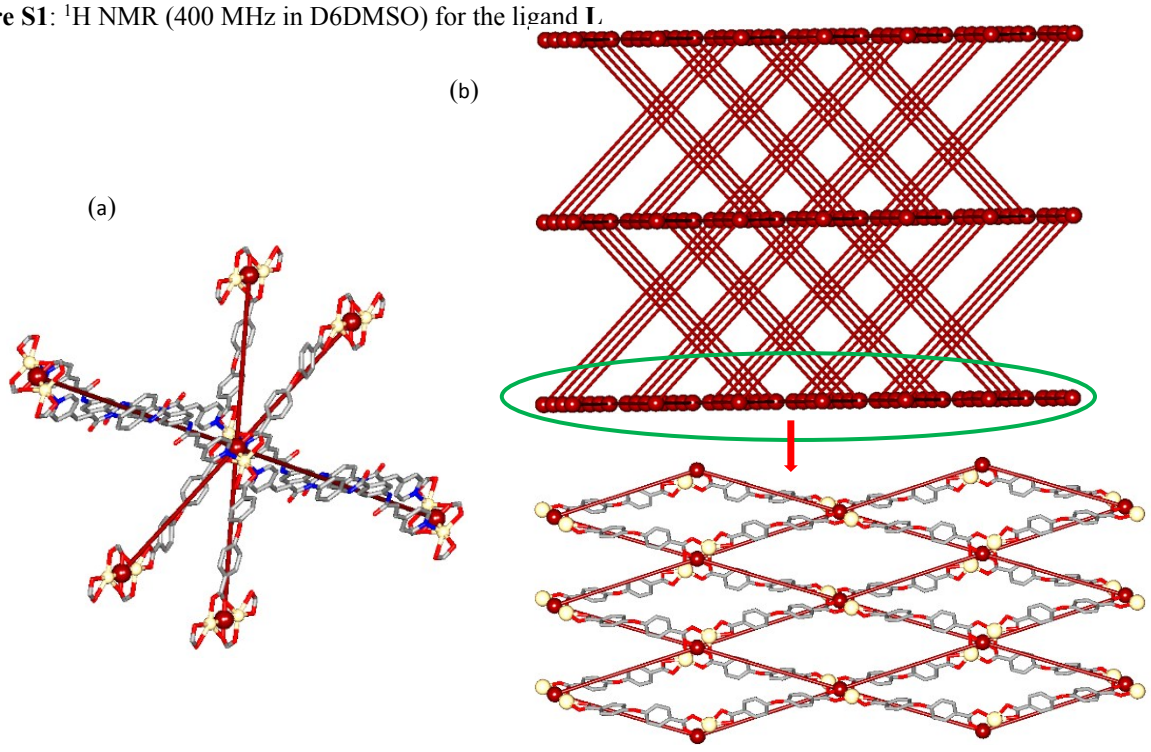

Figure S2: a) six connected node which connects the six neighbouring Cd_2 SBUs (b) 3D-network formed by the pillaring of metal carboxylate 2D layers by **L** units with **mab** topology

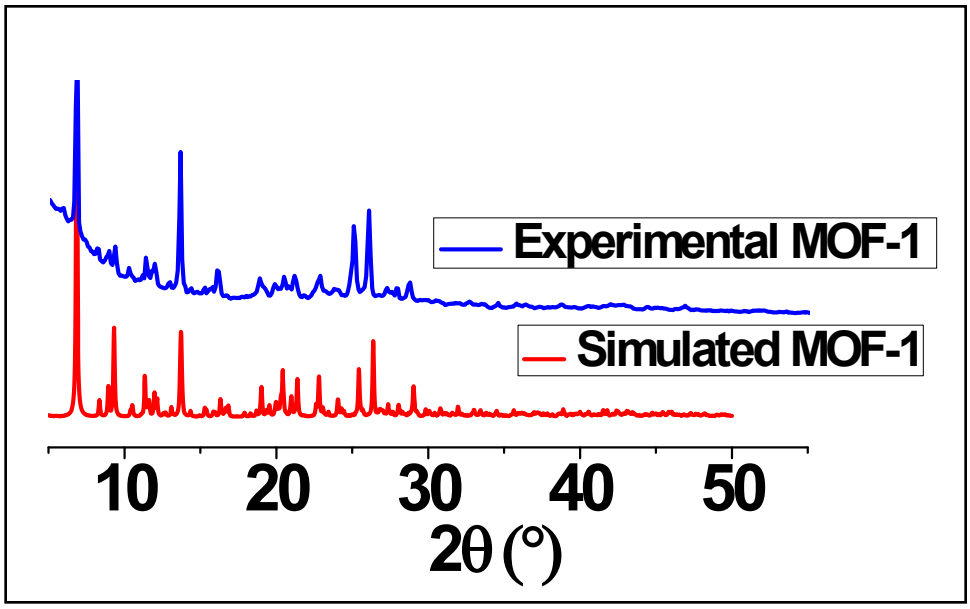

Figure S3: PXRD pattern of simulated and experimental for the MOF-**1**

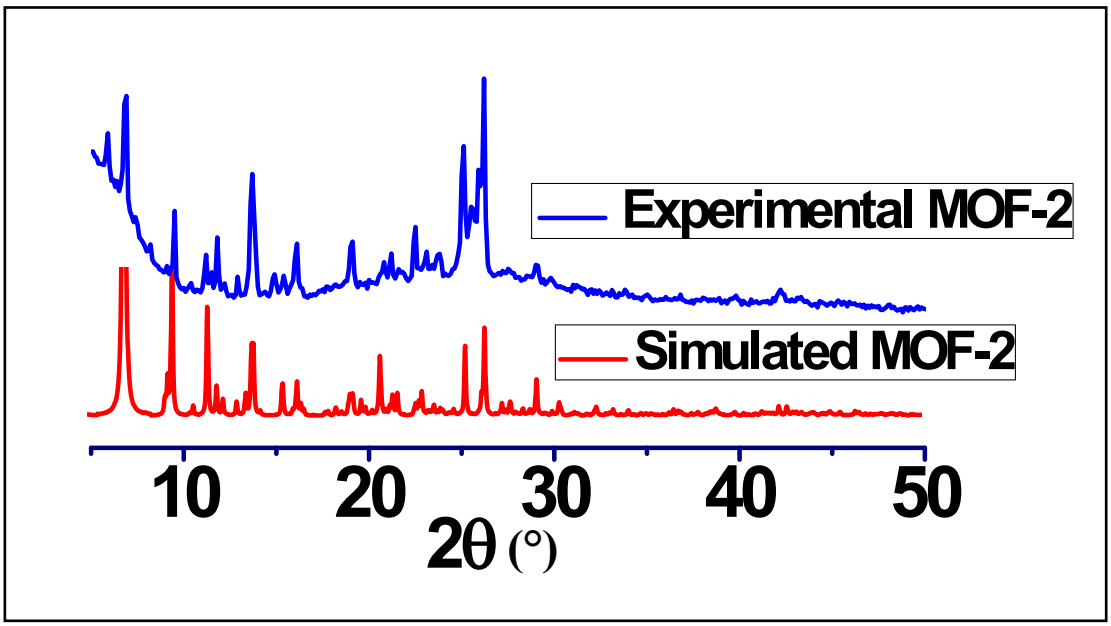

Figure S4: PXRD pattern of simulated and experimental for the MOF-**2**

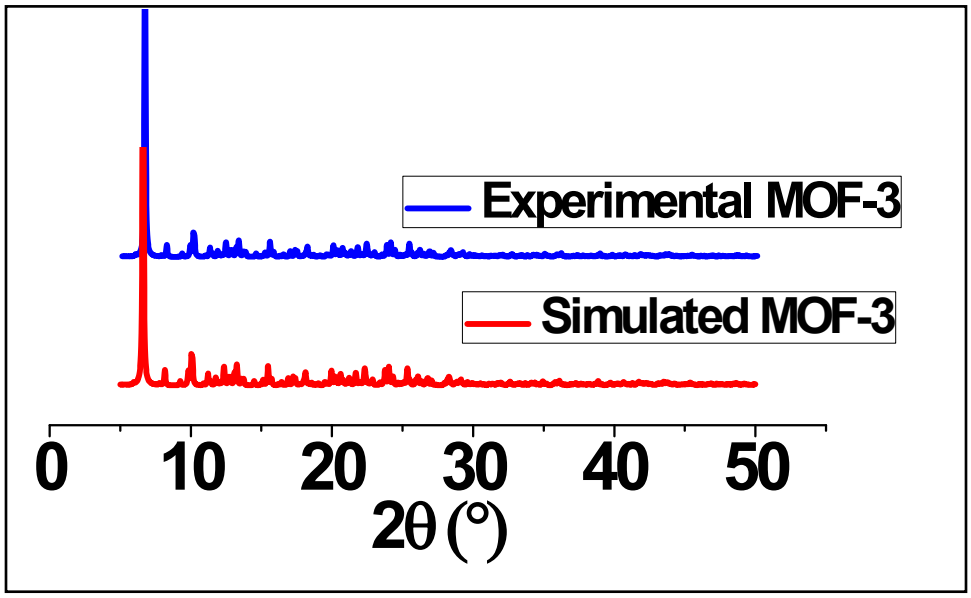

Figure S5: PXRD pattern of simulated and experimental for the MOF-**3**

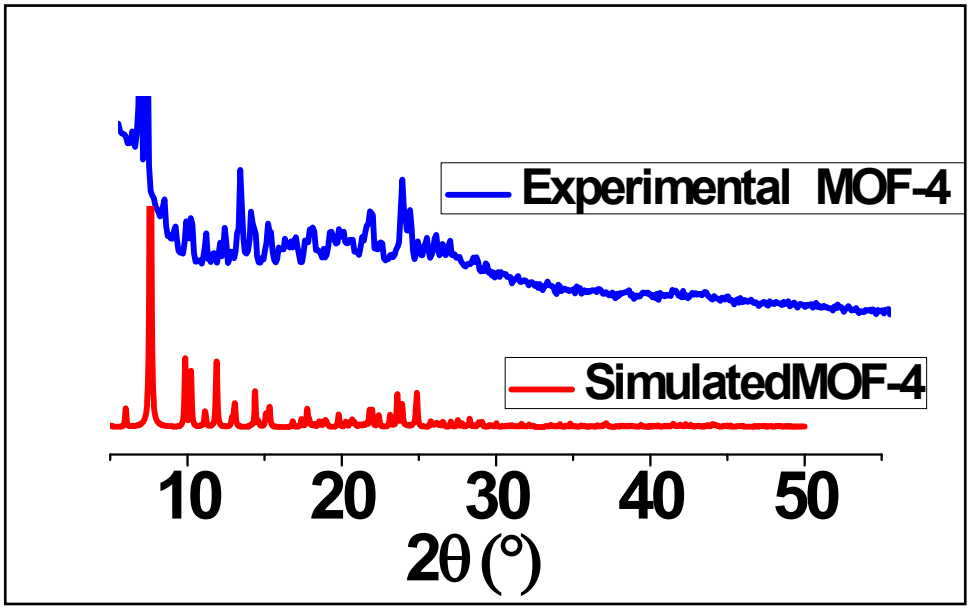

Figure S6: PXRD pattern of simulated and experimental for the MOF-**4**

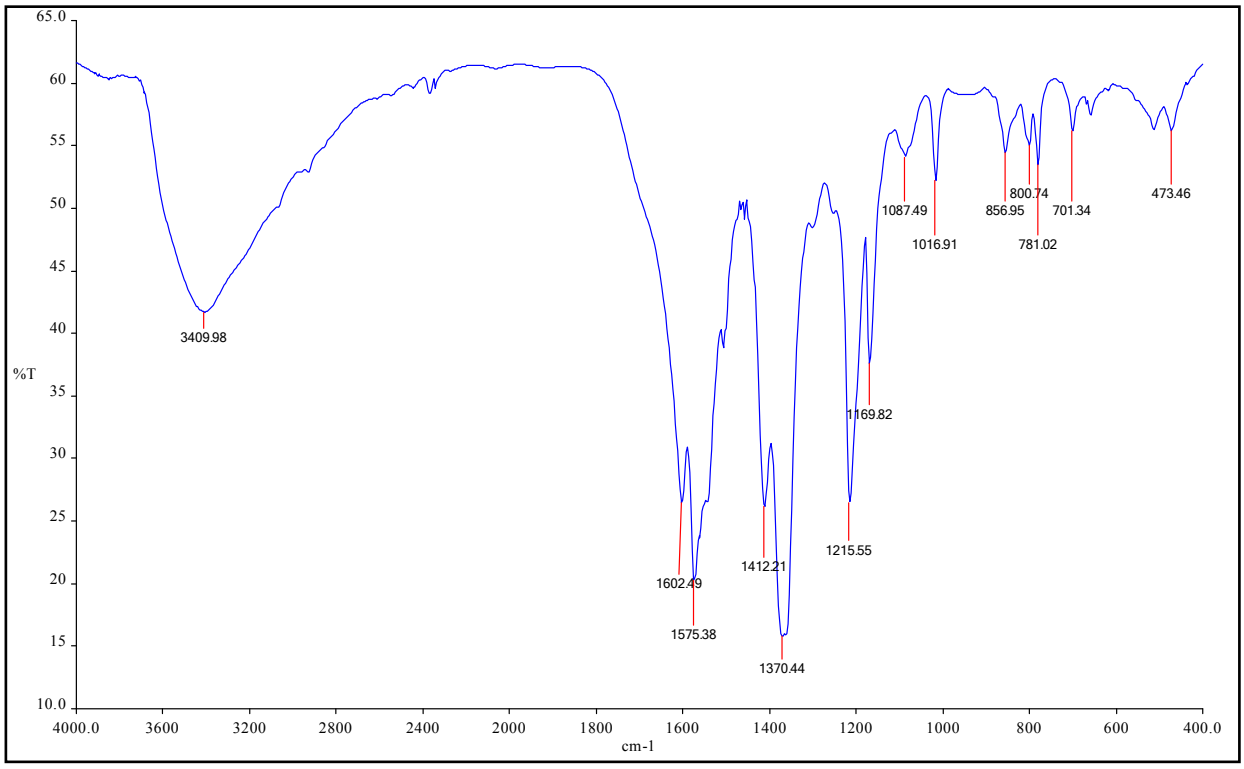

Figure S7: FTIR spectra for ligand **L**

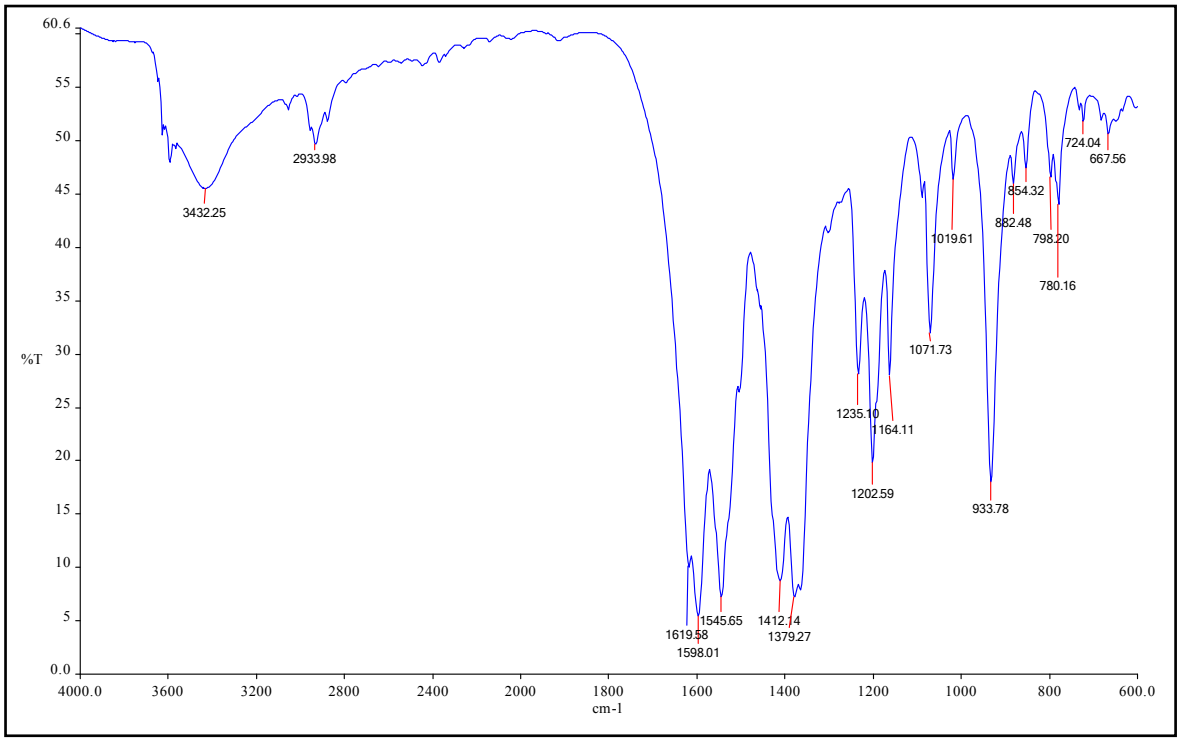

Figure S8: FTIR spectra for the MOF-**1**

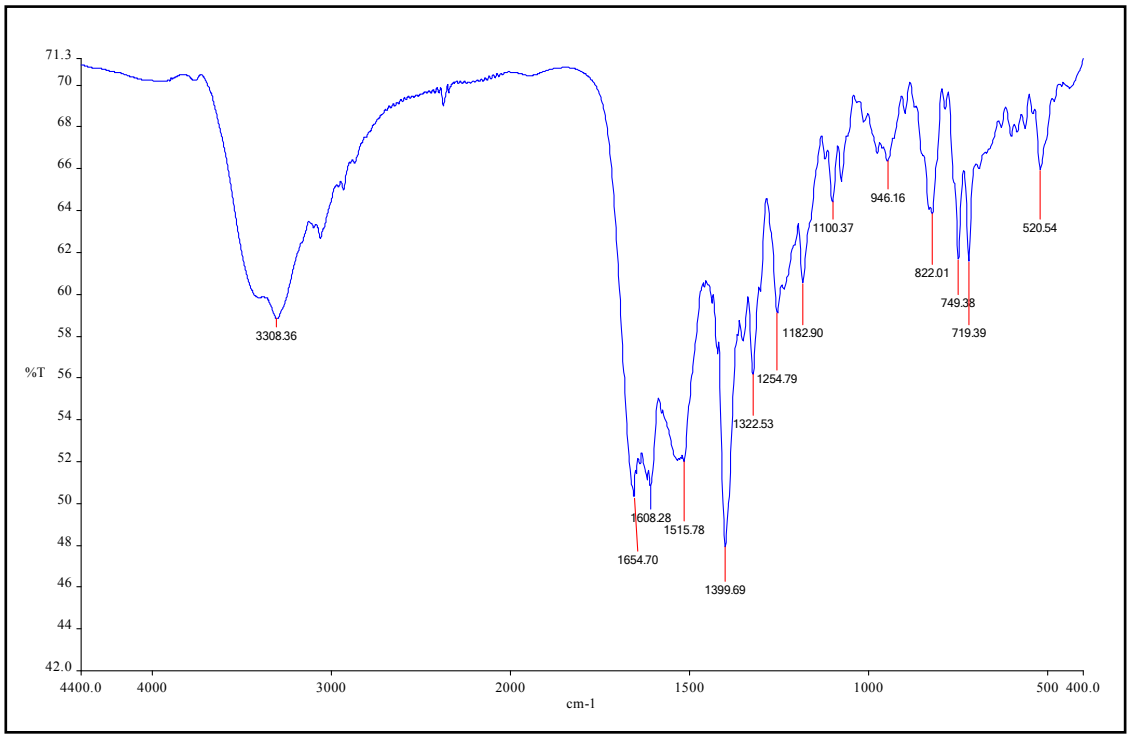

Figure S9: FTIR spectra for the MOF-**2**

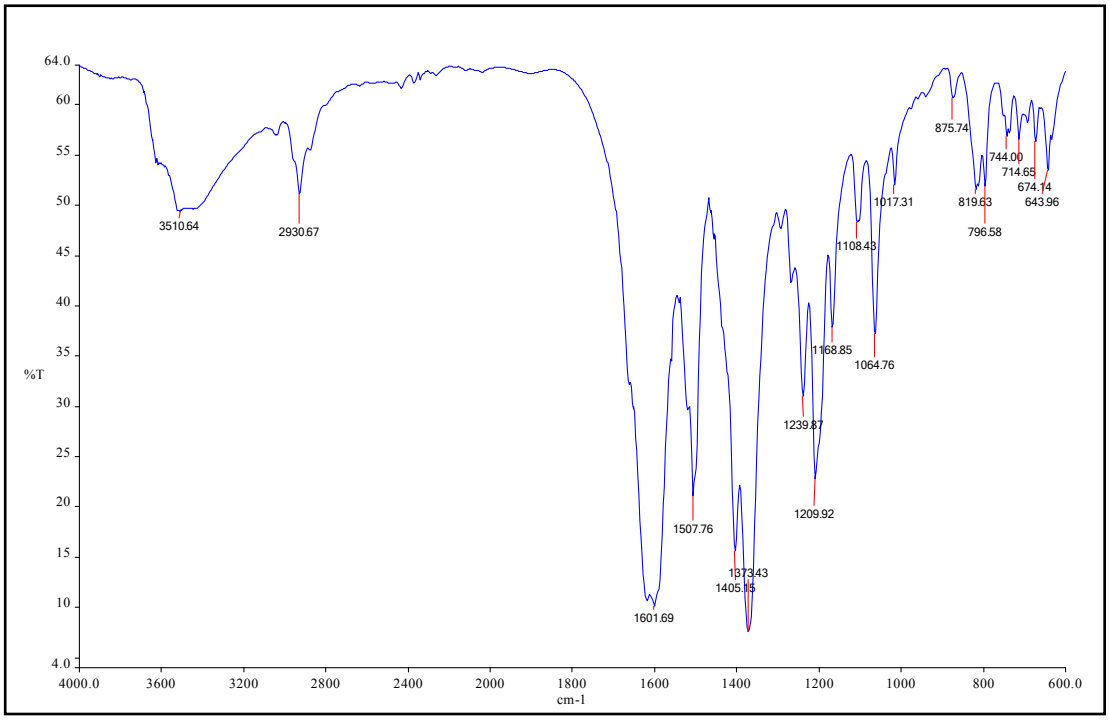

Figure S10: FTIR spectra for the MOF-**3**

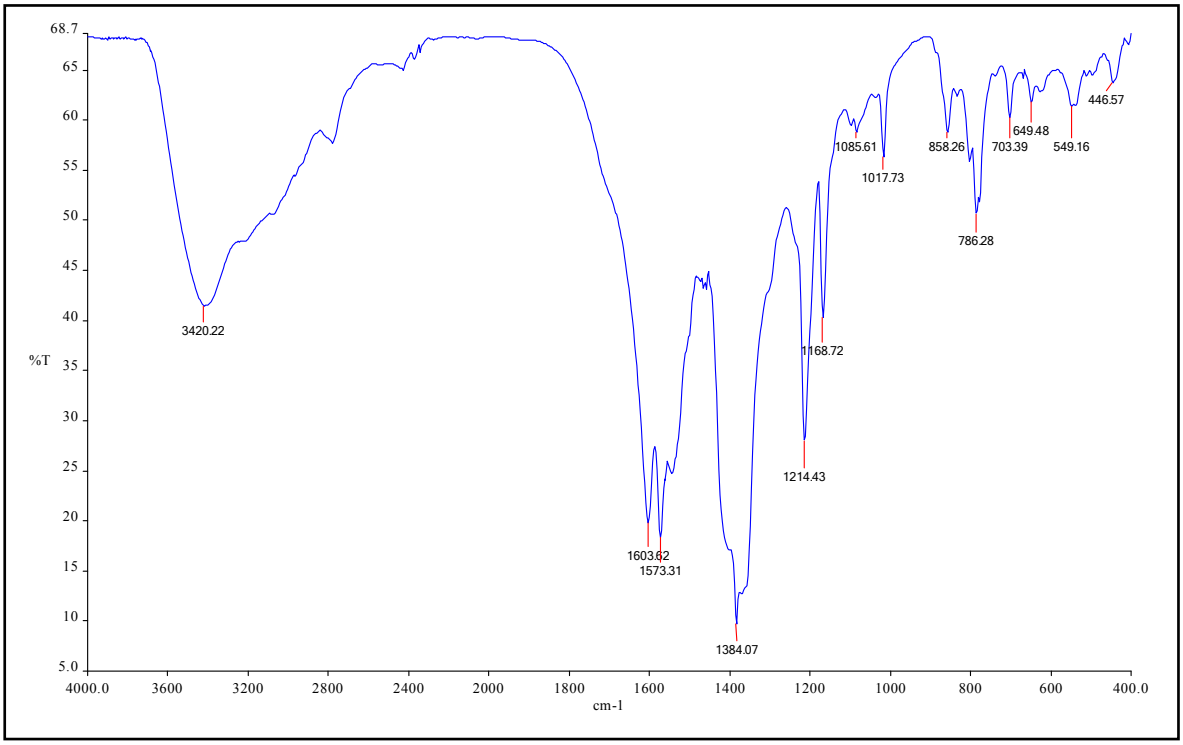

Figure S11: FTIR spectra for the MOF-**4**

To examine the chemical stability and presence of solvent molecules of all the MOFs, TGA was carried out on the powder materials of as synthesized MOF **1-4** with the heating rate of 10 °*C*/min. The TGA curve suggests that the release of guest solvent molecules from MOF-**1** with corresponding weight loss values 28.8 % (cald 28%), up to temperature 120˚*C*. This corresponding weight loss may be attributed to the loss of uncoordinated solvent water molecules and then further weight loss of 8.5% (cald 8%) up to the temperature 320˚*C* is attributed to the one DMF solvent molecule, total framework starts to decompose after that temperature. Similarly, the loss of guest solvent molecules from MOF-**2** with corresponding weight loss 26 % at temperature range 125˚*C* and 6.5% up to temperature 300˚*C* (cald 7%). The corresponding weight loss may be attributed to the loss of thirteen lattice water molecules and one solvent DMF molecule respectively. In case of MOF-**3** the weighty of 20% at temperature range 120˚*C* and 18% (cald 19%) up to the temperature 315˚*C* respectively was observed this weighty may be attributed to loss of eight lattice water and two DMF molecules respectively. The Similar weighty loss of 16 % at temperature 115 ˚*C* and 12% up to 330˚*C* (cald 12.5%) have been observed for the MOF-**4**. The corresponding weight loss

may be attributed to the release of six water and two DMF solvent molecules and the entire framework starts decompose above 330 ˚*C*.

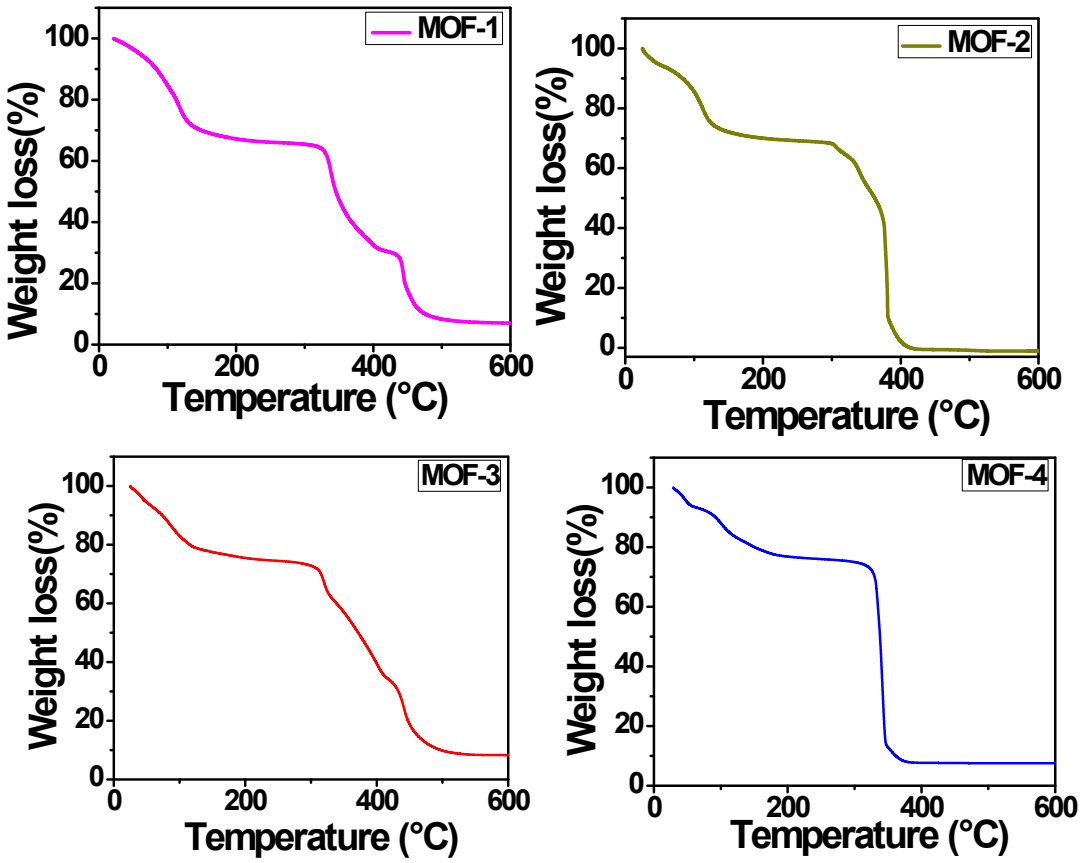

Figure S12: Thermogravimetric analysis graphs for the MOFs **1-4**

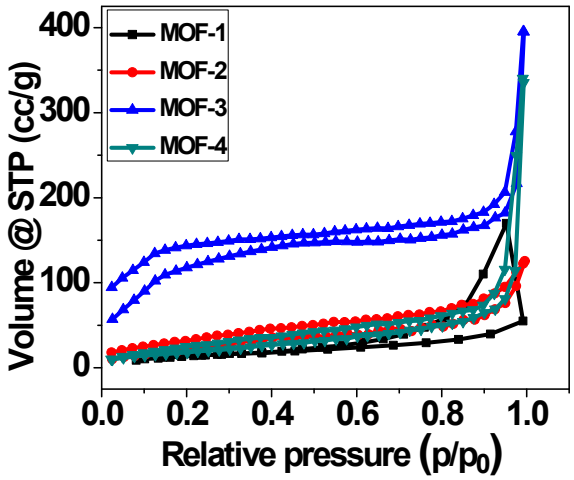

Figure S13: N_2 adsorption and desorption isotherms at 273 K and at one bar for the MOFs **1-4**

Proton Conductivity Study

The impedance behavior of MOFs **1-4** was measured by electrochemical impedance spectroscopy (EIS) using Gamry Instruments, Reference 3000 galvanostat between frequency ranges of 100 Hz to 1 MHz via quasi-two-probe method. In order to measure PC about 100 mg of the freshly prepared samples pressed in a pellet maker to prepare uniform pellets, then further subjected humidification by keeping the pellets in humid chamber for 24h and subsequently measured the proton conductivity. The in-plane proton conductivity (σ) was calculated by using the following equation $\sigma = l/(R \times A)$. Where σ is in-plane proton conductivity in S cm^{-1}, l is the distance between the two electrodes (here, 0.425 cm), R is the measured resistance of the sample and A is an area of the sample i.e., width (cm) × thickness (cm) of the sample. The proton conductivity of MOFs at different humidity was measured using a HSA™ humidifier unit and an FC-25-01-BT Conductivity Cell from ElectroChem, Inc.

The proton conductivity of all the MOFs **1-4** at 80 °*C* and at different relative humidity conditions have been shown below.

MOF-**1**

$\sigma = 1.2 \times 10^{-3}$ S cm^{-1}at 98% RH

$\sigma = 6.6 \times 10^{-4}$ S cm^{-1} at 80% RH

$\sigma = 4.3 \times 10^{-4}$ S cm^{-1} at 70% RH

$\sigma = 1.3 \times 10^{-4}$ S cm^{-1} at 60% RH

$\sigma = 4.7 \times 10^{-4}$ S cm^{-1} at 50% RH

MOF-**2**

$\sigma = 9.5 \times 10^{-4}$ S cm^{-1}at 98% RH

$\sigma = 1.7 \times 10^{-4}$ S cm^{-1} at 80% RH

$\sigma = 7.0 \times 10^{-5}$ S cm^{-1} at 70% RH

$\sigma = 2.0 \times 10^{-5}$ Scm^{-1} at 60% RH

$\sigma = 9.7 \times 10^{-6}$S cm^{-1} at 50% RH

MOF-**3**

$\sigma = 2.2 \times 10^{-3}$ S cm^{-1} at 98% RH

$\sigma = 1.0 \times 10^{-3}$ S cm^{-1} at 80% RH

$\sigma = 6.8 \times 10^{-4}$ S cm^{-1} at 70% RH

$\sigma = 5.7 \times 10^{-4}$ S cm^{-1} at 60% RH

$\sigma = 4.5 \times 10^{-4}$ S cm^{-1} at 50% RH

MOF-**4**

$\sigma = 6.6 \times 10^{-4}$ S cm^{-1}at 98% RH

$\sigma = 4.8 \times 10^{-4}$ S cm^{-1} at 80% RH

$\sigma = 2.1 \times 10^{-4}$ S cm^{-1} at 70% RH

$\sigma = 1.2 \times 10^{-4}$ S cm^{-1} at 60% RH

$\sigma = 4.6 \times 10^{-6}$ S cm^{-1} at 50% RH

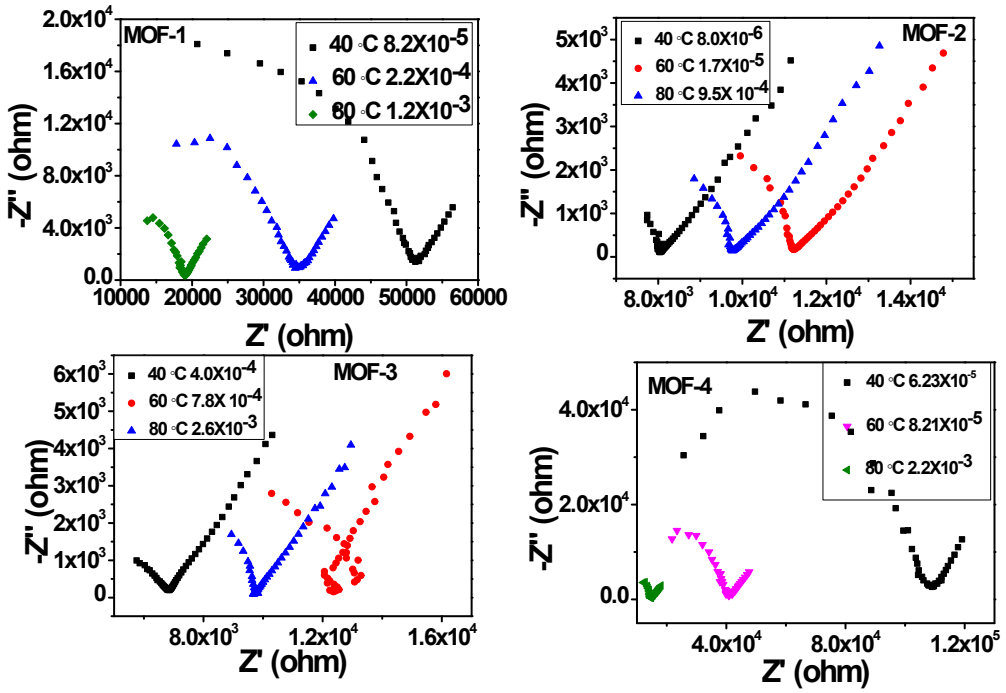

Figure S14: Nyquist plots for the MOFs **1-4** at 40, 50 and 60 °*C* temperature respectivily and at 98% (RH).

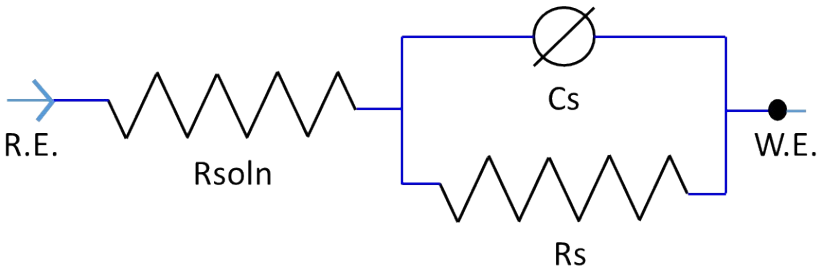

Where R.E. reference electrode

W.E. working electrode

R soln solution resistance

R_s sample resistance in bulk phase for proton conduction

C_s constant phase element of sample corresponds to rate determining process

Figure S15: Equivalent circuit model diagram for the impedance measurement of the MOFs **1-4**

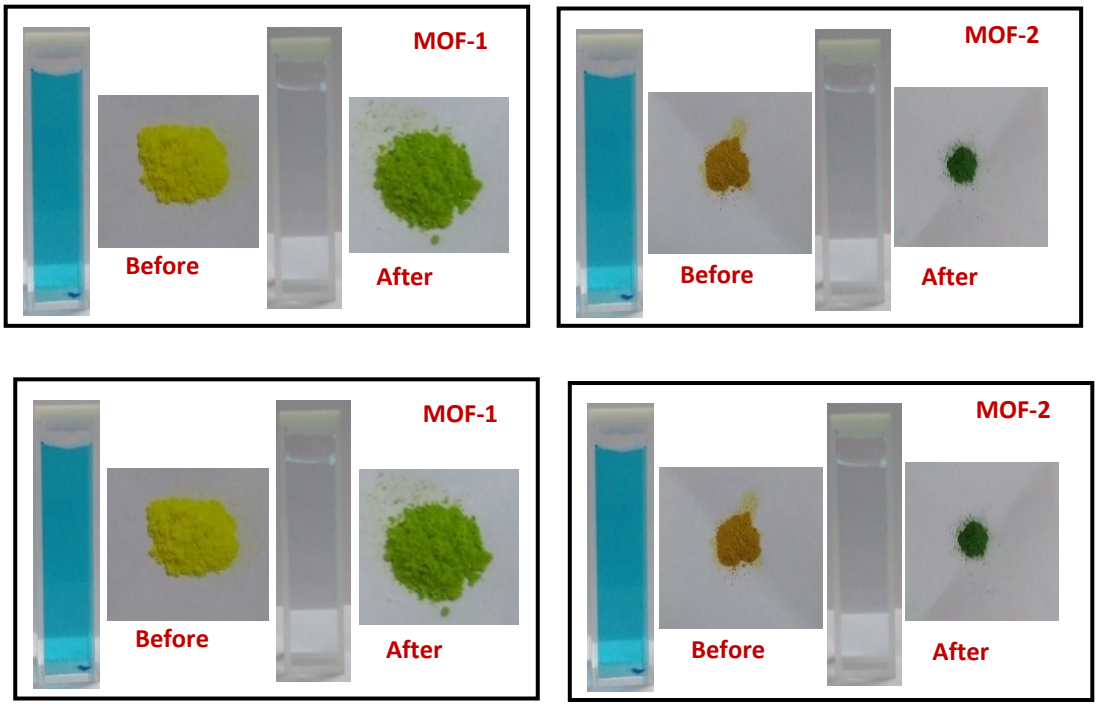

Figure S16: Illustration for the change in the color of the material after Methylene blue dye adsorption by MOFs **1-4** in aqueous solution

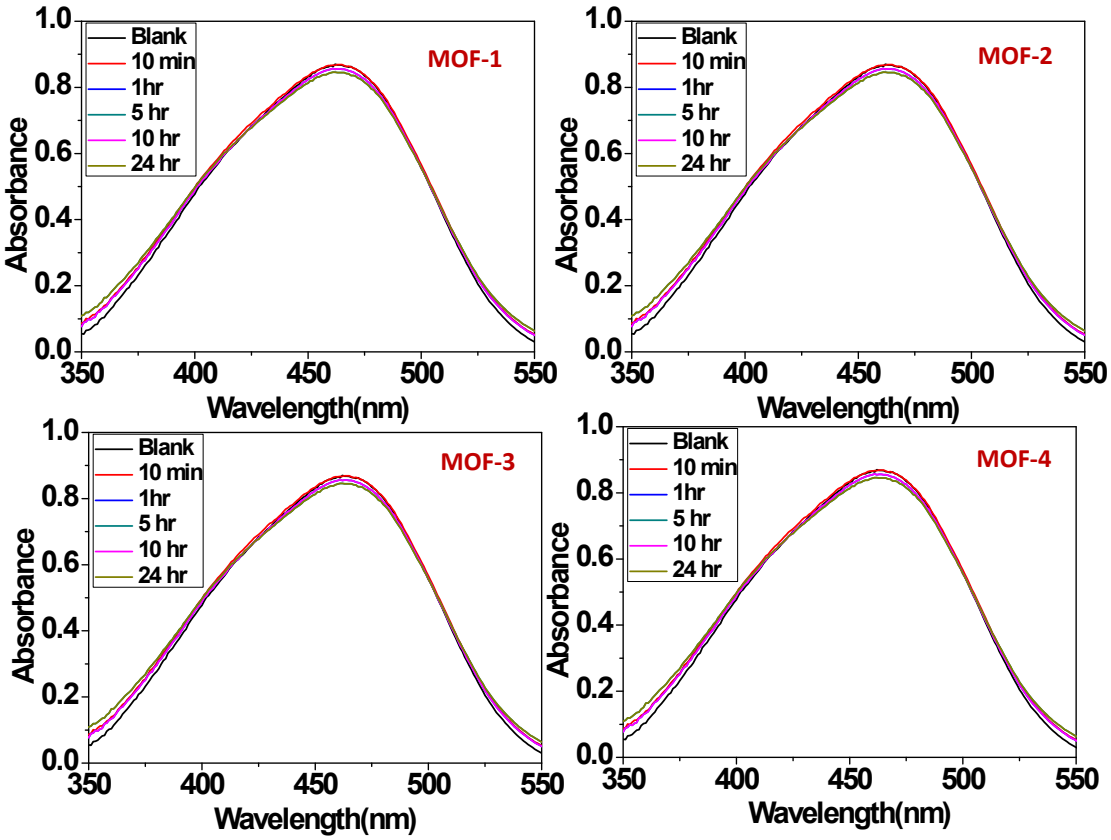

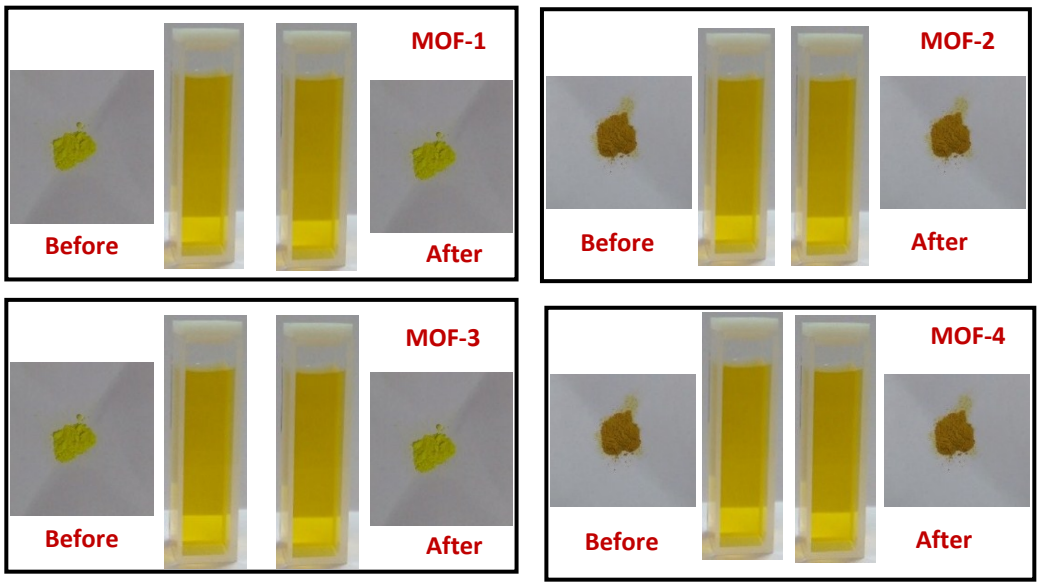

Figure S17: UV-vis spectra for the zero uptake of methyl orange from aqueous solutions at various time intervals for the MOFs **1**-**4**.

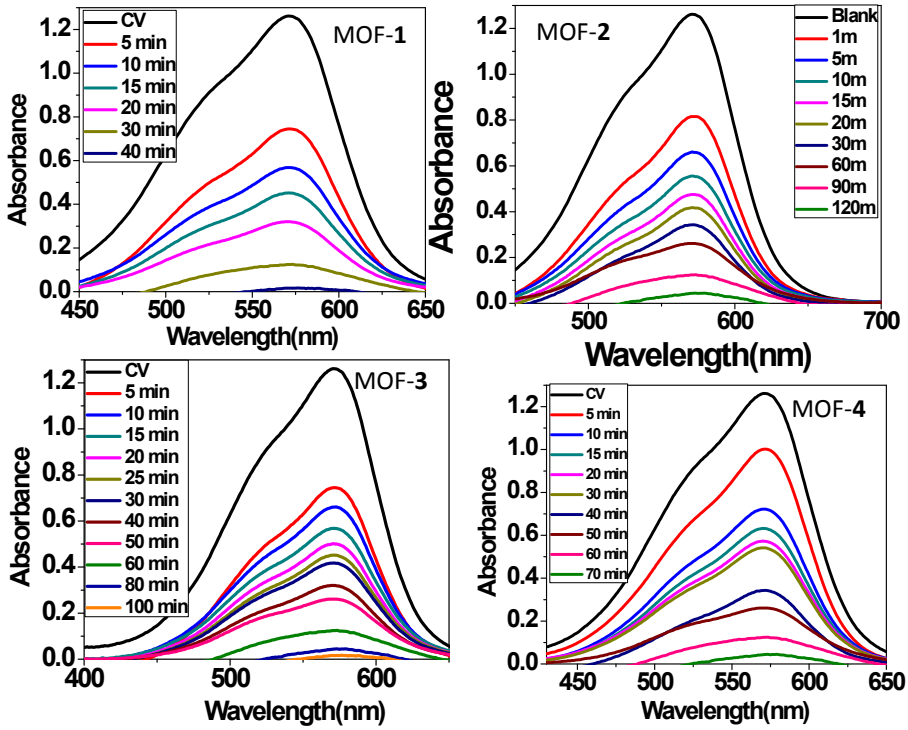

Figure S18: UV-vis spectra for the uptake of crystal violet from aqueous solutions at various time intervals for MOFs **1**-**4** respectivily.

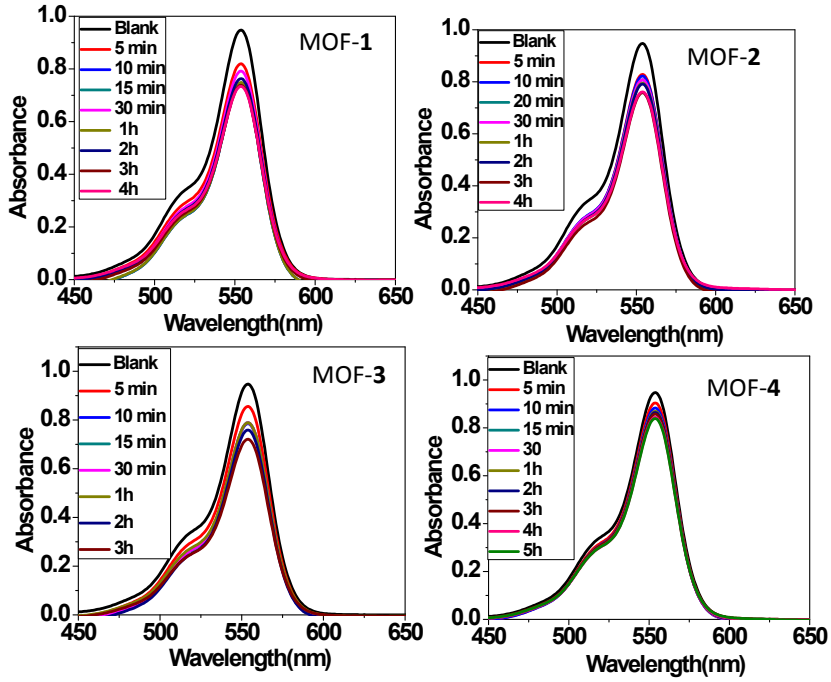

Figure 19: UV-vis spectra for the very low uptake of rhodamine B from aqueous solutions at various time intervals for MOFs **1**-**4** respectivily.

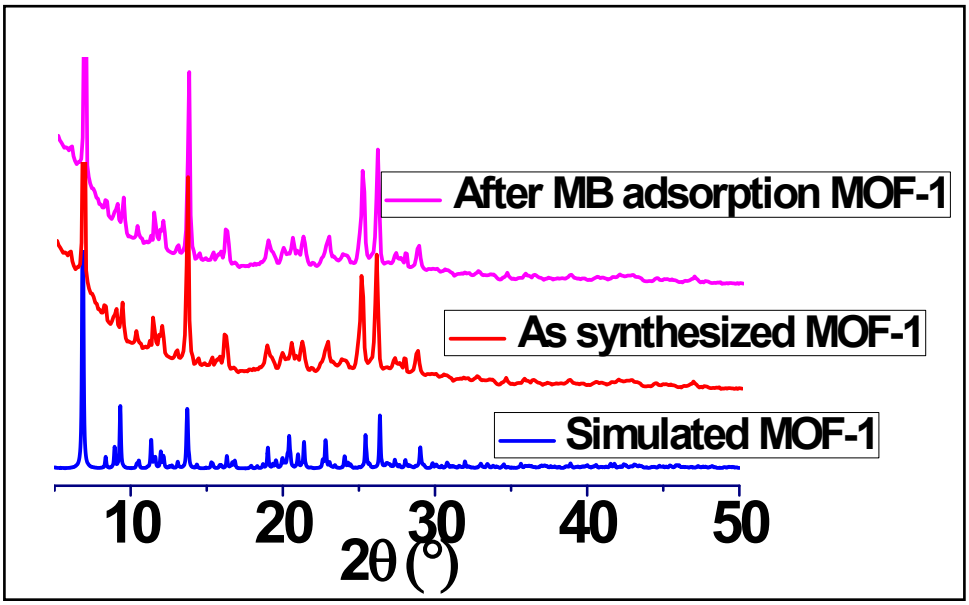

Figure S20: Comparison of PXRD patterns for MOF-**1** after dye adsorption

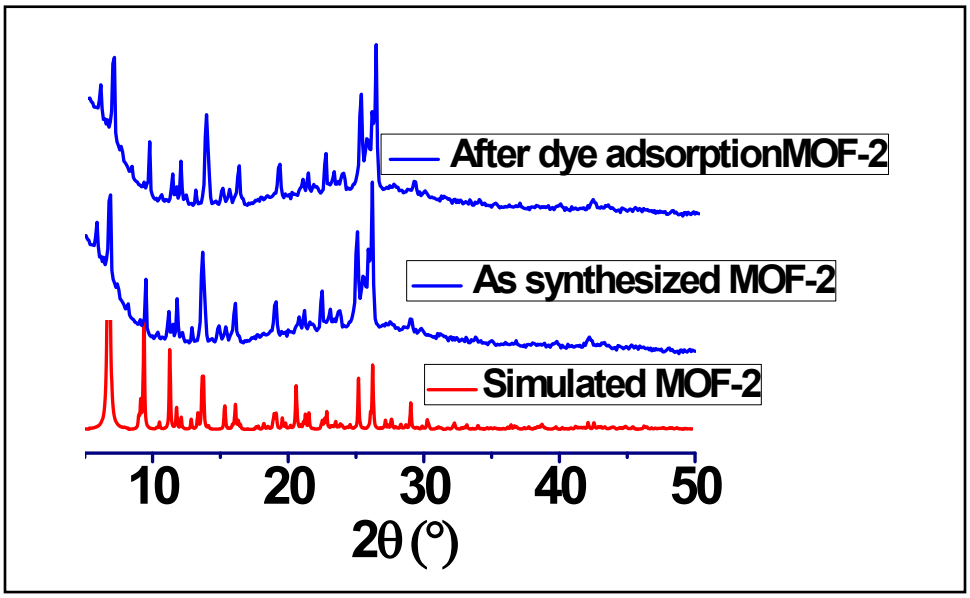

Figure S21: Comparison of PXRD patterns for MOF-**2** after dye adsorption

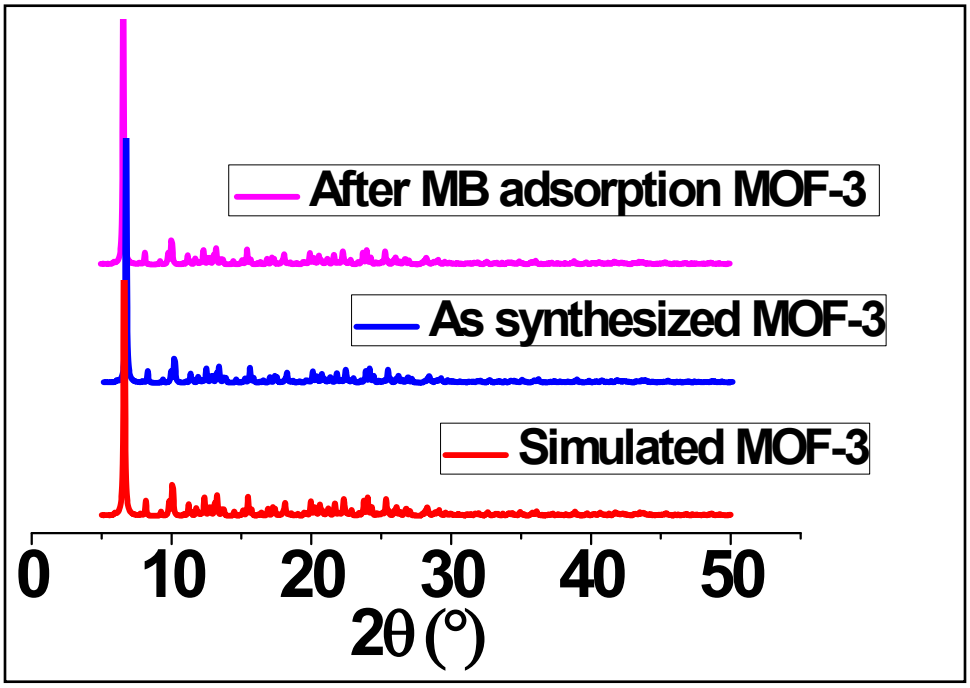

Figure S22: Comparison of PXRD patterns for MOF-**3** after dye adsorption

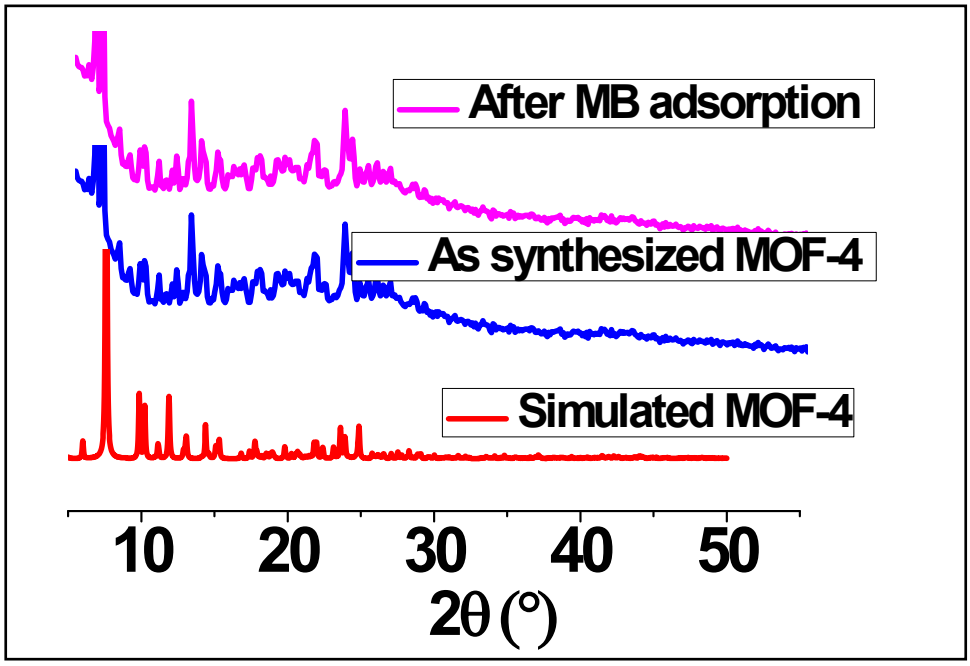

Figure S23: Comparison of PXRD patterns for MOF-**4** after dye adsorption

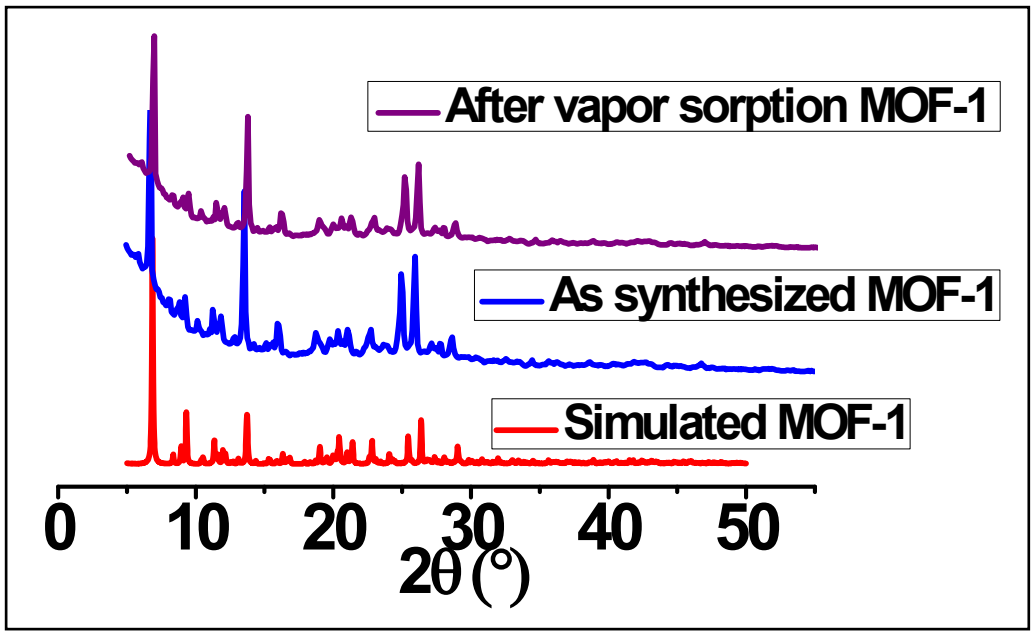

Figure S24: Comparison of PXRD patterns for MOF-**1** before and after vapor sorption.

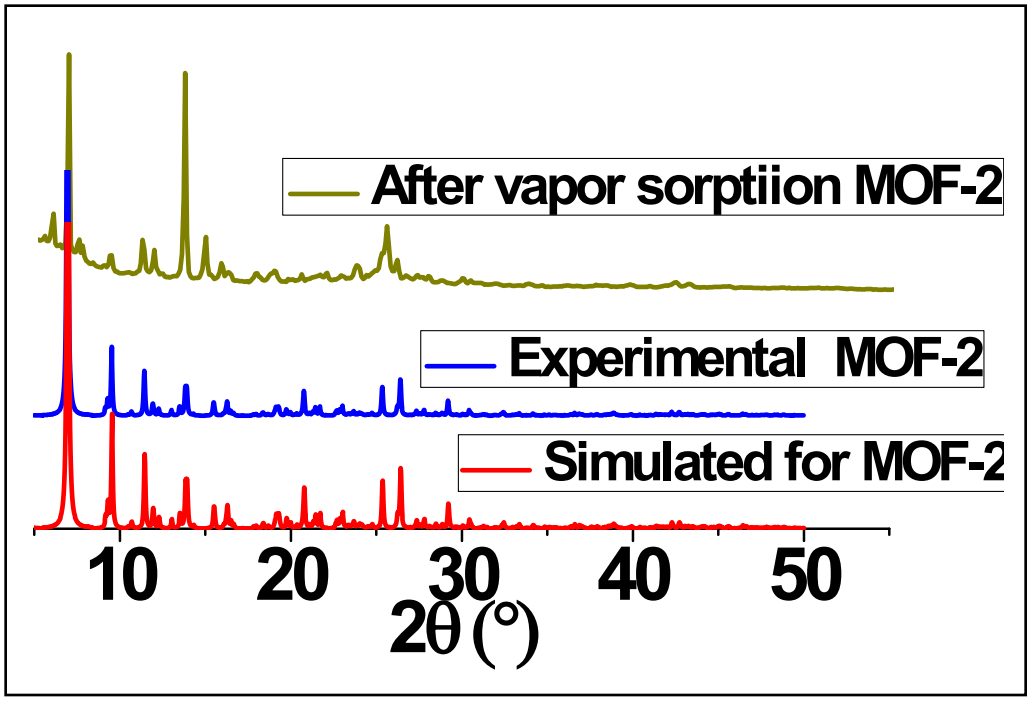

Figure S25: Comparison of PXRD pattern of MOF-**2** before and after vapor sorption.

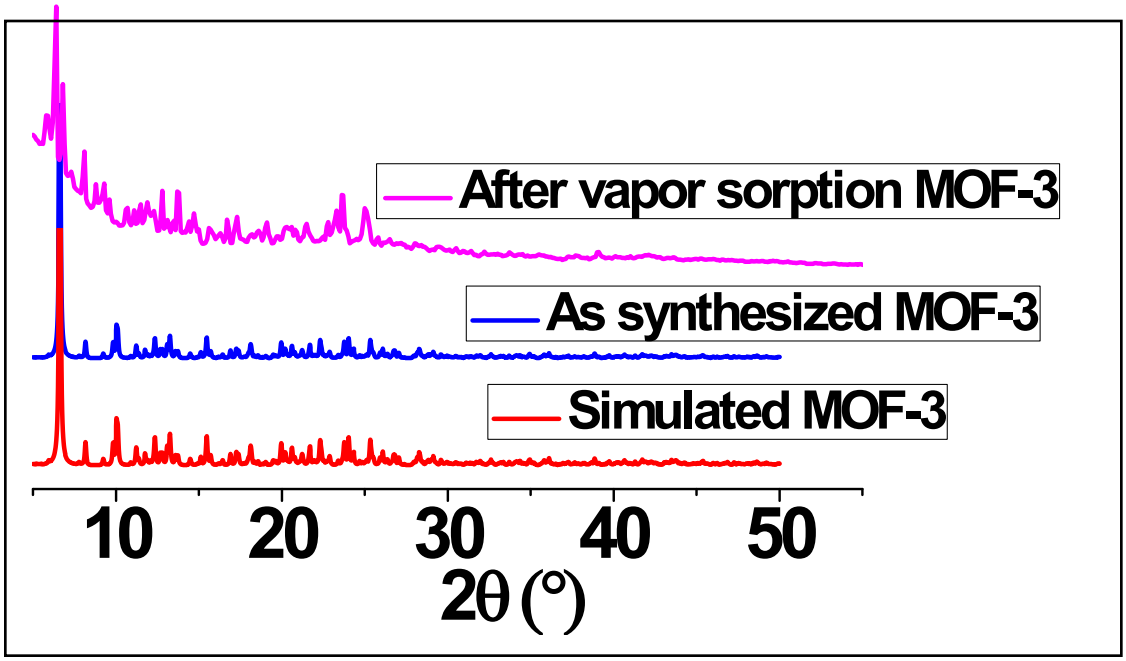

Figure S26: Comparison of PXRD patterns of MOF-**3** before and after vapor sorption.

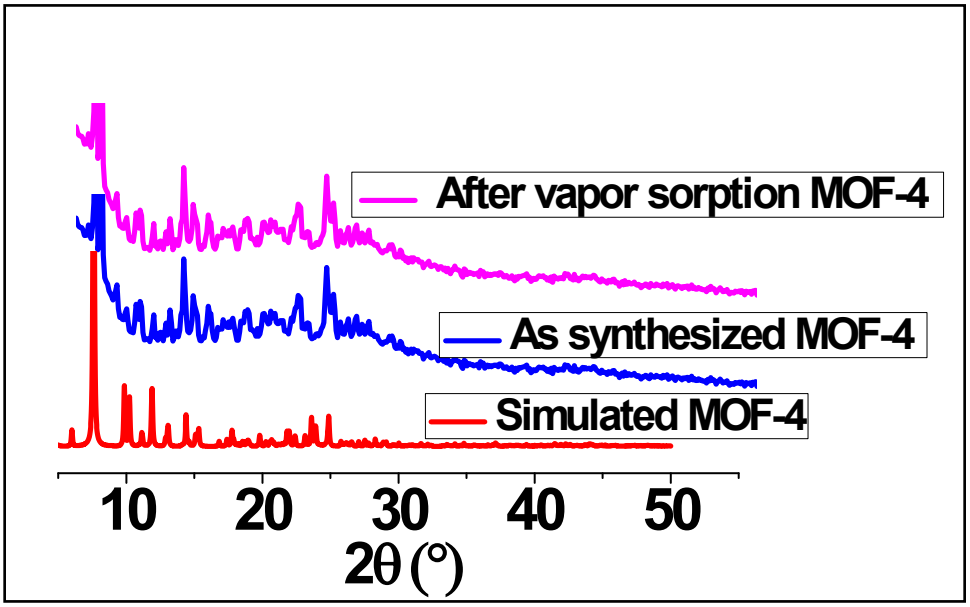

Figure S27: Comparison of PXRD patterns of MOF-**4** before and after vapor sorption.

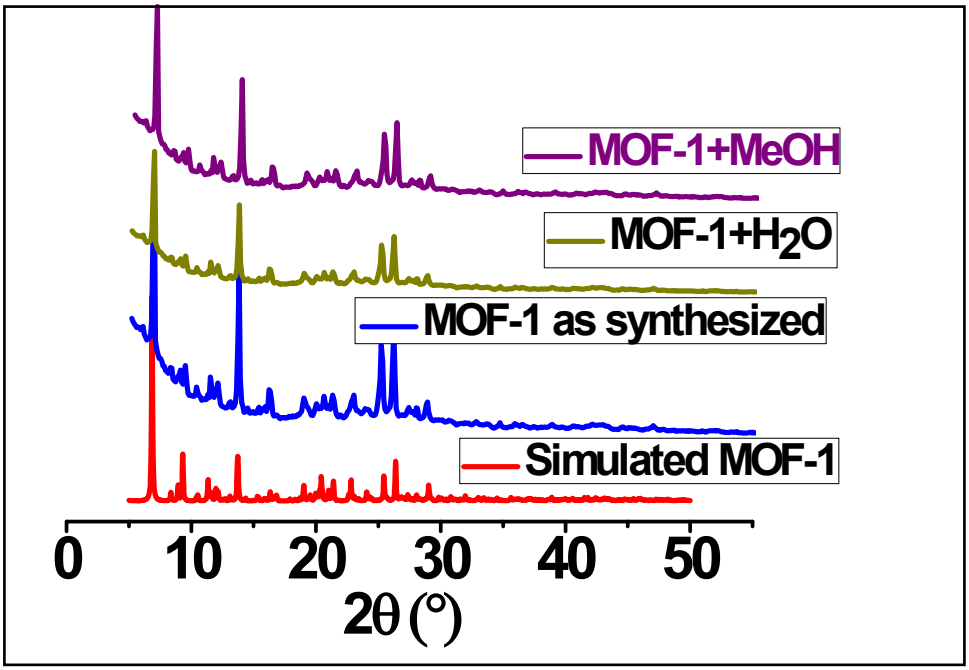

Figure S28: Comparison of PXRD patterns of MOF-**1** in different solvents.

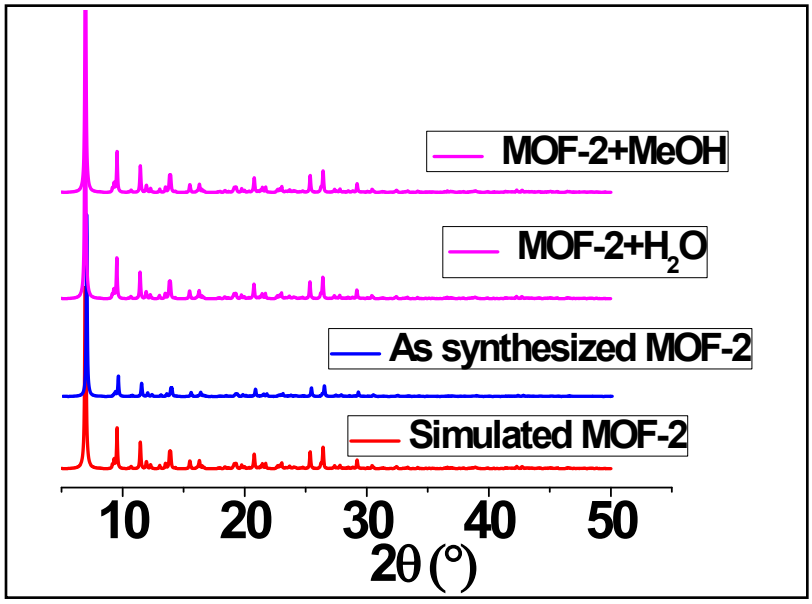

Figure S29: Comparison of PXRD patterns of MOF-**2** in different solvents.

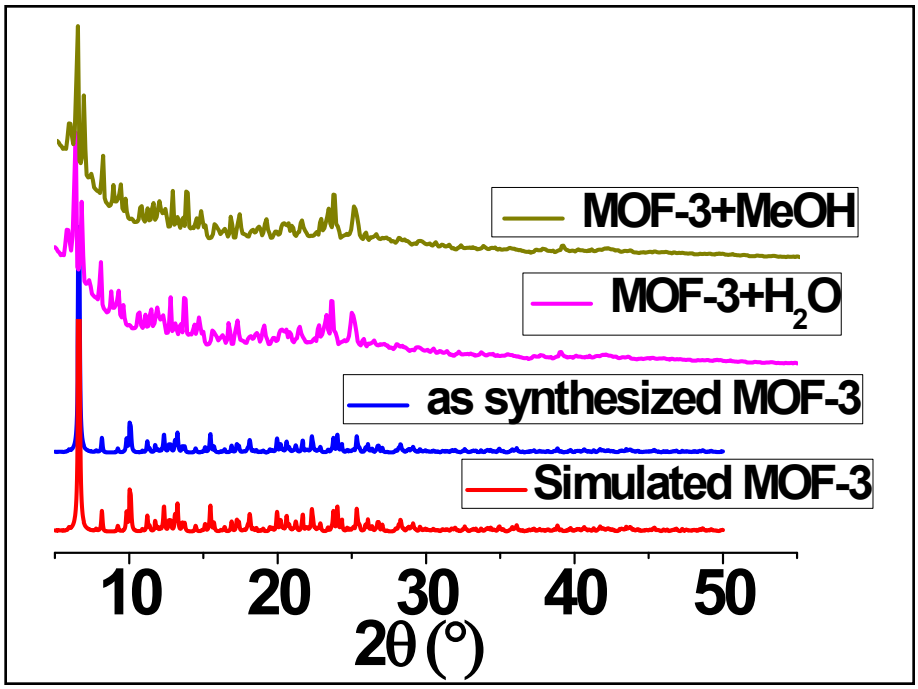

Figure S30: Comparison of PXRD patterns of MOF-**3** in different solvents

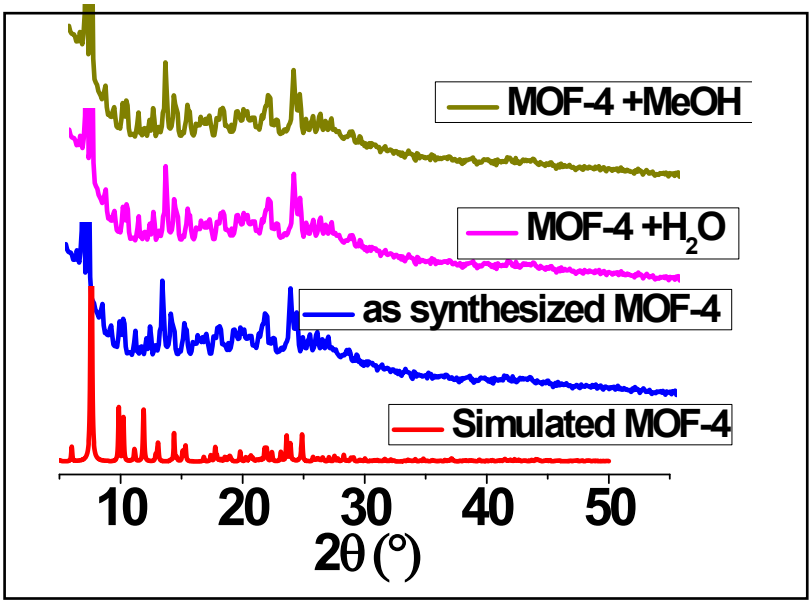

Figure S31: Comparison of PXRD patterns of MOF-**4** in different solvents.

Table S1: Geometrical parameters of hydrogen bonds in MOF **1-4**

MOF number	Type of Hydrogen bond	H···A (Å)	D···A (Å)	D-H···A (°)
MOF-**1**	N-H ···O	2.03	2.871(6)	166
	N-H ···O	2.29	3.026(13)	144
	N-H ··O	2.18	2.996(11)	158
	C-H ··O	2.60	3.488(17)	160
	C-H ··O	2.48	3.307(14)	149
MOF-**2**	N-H ··O	2.18	3.006(5)	160
	N-H ··O	2.33	3.119(8)	153
	N-H ··O	2.01	2.856(4)	169
	C-H ··O	2.51	3.057(4)	118
MOF-**3**	N-H ··O	2.07	2.924(7)	170
	N-H ··O	2.09	2.928(17)	163
	N-H ··O	2.01	2.855(14)	169
	C-H ··O	2.56	3.447(10)	154
MOF-**4**	N-H···O	2.07	2.924(7)	170
	N-H ··O	2.09	2.928(17)	163
	N-H ··O	2.01	2.855(14)	169
	C-H ··O	2.56	3.447(10)	154

Table-2. Comparison of water vapor sorption values with existing literature.

Coordination polymers or MOF	Water sorption value	Reference
Pillared-Layer Coordination Polymers {[Cd(pzdc)(azpy)]·2 H_2O}$_n$ and {[Cd(pzdc)(bpee)]·1.5H_2O}$_n$	~80 cc/g	*Angew. Chem. Int., Ed*. **2004**, *43*, 3269-3272.
3D-framework {[Gd_2(dhbdc)(dhbdcH_2)(H_2O)$_5$]}$_n$	~ 60 ml/g	*Cryst. Growth Des.* **2009***, 9,* 3844-3847.
ZIF-8, MIL-100, MIL-101, DUT-4	~ 165-1600 cc/g	*Microporous Mesoporous* *Mater*. **2009**, *120*, 325-330.
2D-noninterpenetrated flexible metal-organic porous solid, {[Cu_2(cis-chdc)2(bpee)] 3 H_2O}$_n$	~60 ml/g	*Inorg. Chem*. **2009**, *48*, 10886-10888.
2D- layers [{Zn(5-NO_2-ip)(bpy)}(0.5DMF·0.5MeOH)]$_n$ [{Zn(5-MeO-ip)(bpy)}(0.5DMF·0.5MeOH)]$_n$	~4 or 5 water molecules per unit cell	*Angew. Chem. Int. Ed*., **2010**, *49*, 4820-4824.
Pillared-bilayer 2D- CP {[Cd4(azpy)$_2$-(pyrdc)4(H_2O)$_2$] 9H_2O}$_n$	~100 cc/g	*Chem. Commun.,* **2011***, 47,* 8106-8108.
Metal Organic Frameworks with Unprecedented Zeolitic unh-Topology	~6-12 wt%	*J. Am. Chem. Soc*. **2011**, *133*, 17950-17958.
UiO-66, UiO-66(NH_2), UiO-66(NO_2), UiO-66(2,4 (OMe)$_2$)	~ 10-25 mol/kg	*Langmuir* **2012**, *28*, 15606-15613.
2D structure, DUT-84	~150 cc/g	*CrystEngComm*. **2013**, *15*, 9572-9577.

Flexible ultramicroporous Co based MOF, $[Co1.5(tipb)\ (SO_4)(bdc)0.5]_n$	~ 250 cc/g	*Angew. Chem., Int., Ed.,* **2013***,* *52,* 11550.
CAU-10 (-NO_2, -NH_2, -CH_3, -OCH_3, and -OH groups).	~100-400 cc/g	*Chem. Mater*, **2013**, *25*, 17.
2D pillared-bilayer MOF $\{[Cu(tdc)(bpe)]n\cdot 2n(H_2O)\cdot n(MeOH)\}$	~160 cc/g	*Dalton Trans*. **2014**, *43*, 7191-7199.
3D Metal-organic Frameworks $\{[Cd(NH_2\text{-}bdc)(bpe)]\cdot 0.5EtOH\}_n$ and $\{[Cd(NO_2\text{-}bdc)(azbpy)]\cdot 4H_2O\}_n$	~50-180 cc/g	*CrystEngComm*, **2014**, *16*, 4877-4885.
MOF-801-SC (single crystal form),-802,-805, -806, -808, -812, and -841, MOF-801-P, MOF-812, MOF-801-P and MOF-841	~100-800 cc/g	*J. Am. Chem. Soc*. **2014**, *136*, 4369-4381.
3D-l microporous framework, Zn(II)-MOF $[Zn(HPyImDC)(DMA)]_n$	~ 90 cc/g	*Dalton Trans.,* **2014**, *43*, 8311-8317.
$[Cu_3(TTPB)2\ (H_2O)6]\cdot 5DMF$ (JUC-130) and $[Cd_3(TTPB)2(H_2O)6]\cdot 6DMF$ (JUC-131)	~150 cc/g	*Cryst. Growth Des.* **2015***, 15,* 2033-2038.
Polyhedral-Based 3D-Metal-Organic Frameworks $\{[Ni(BTC)0.66(BPz)_2]\cdot 2MeOH\cdot 4H_2O\}_n$, $\{[Co(BTC)0.66\text{-}(BPz)_2]\cdot 2MeOH\cdot 4H_2O\}_n$, $\{[Mn(BTC)0.66(BPz)_2]\cdot 2MeOH\cdot 4H_2O\}_n$	~350 cc/g	Cryst. Growth Des. **2015,** *15,* 2732-2741.
Our results	195-330 cc/g	This work

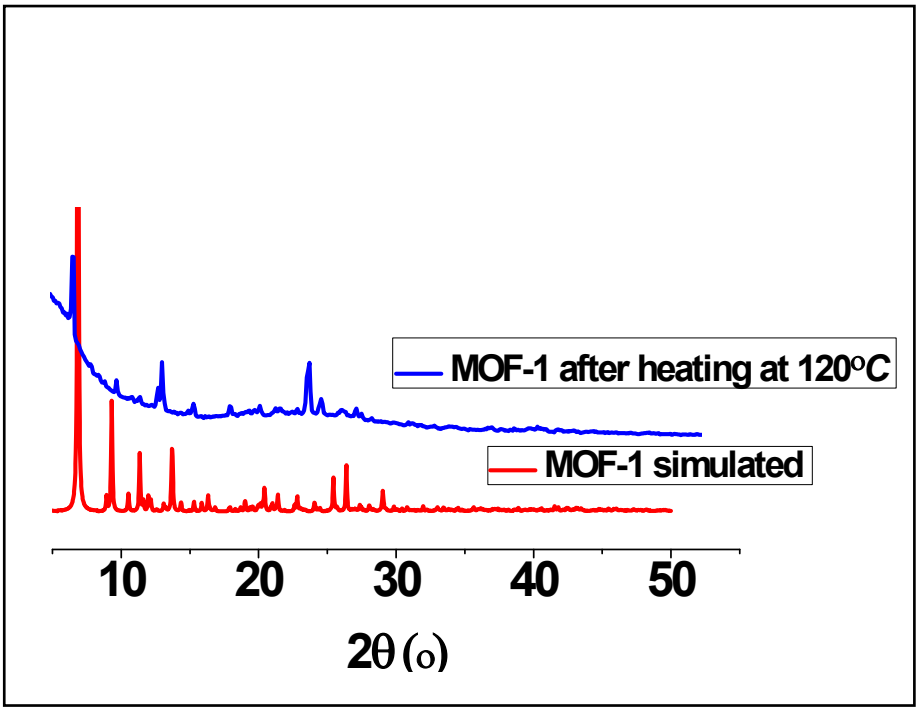

Figure S32: Comparison of PXRD patterns of MOF-**1** after heat treatment.

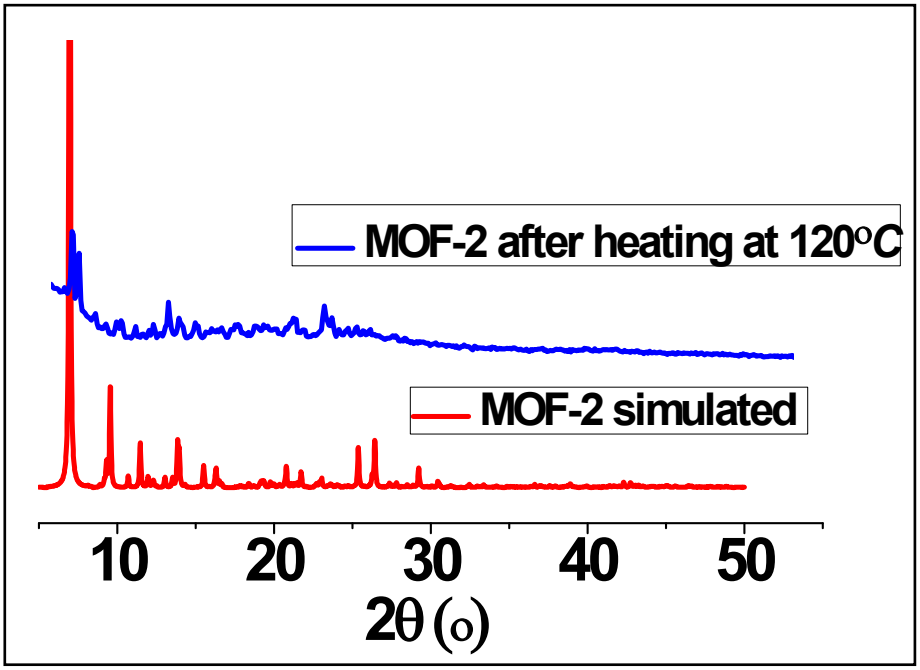

Figure S33: Comparison of PXRD patterns of MOF-**2** after heat treatment.

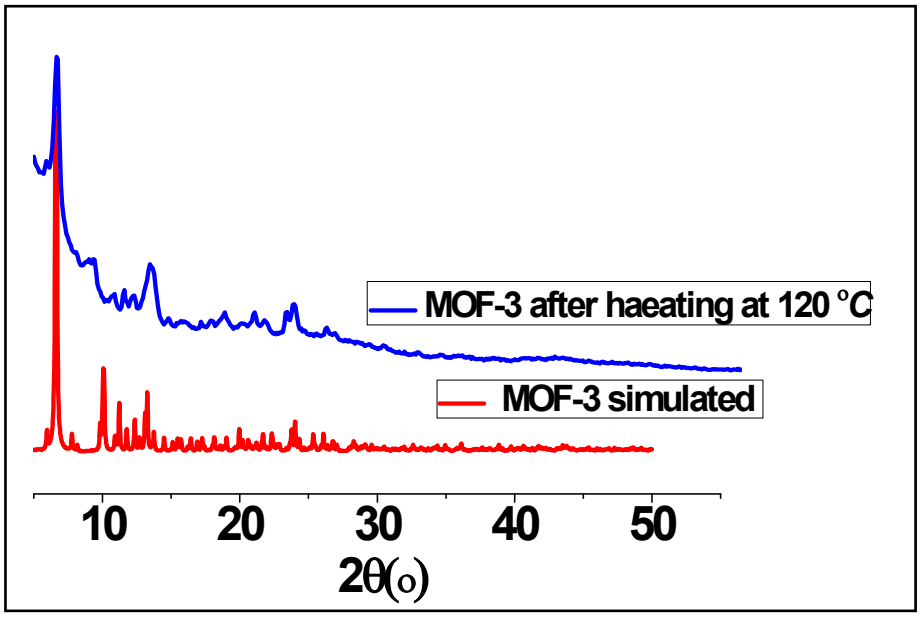

Figure S34: Comparison of PXRD patterns of MOF-**3** after heat treatment

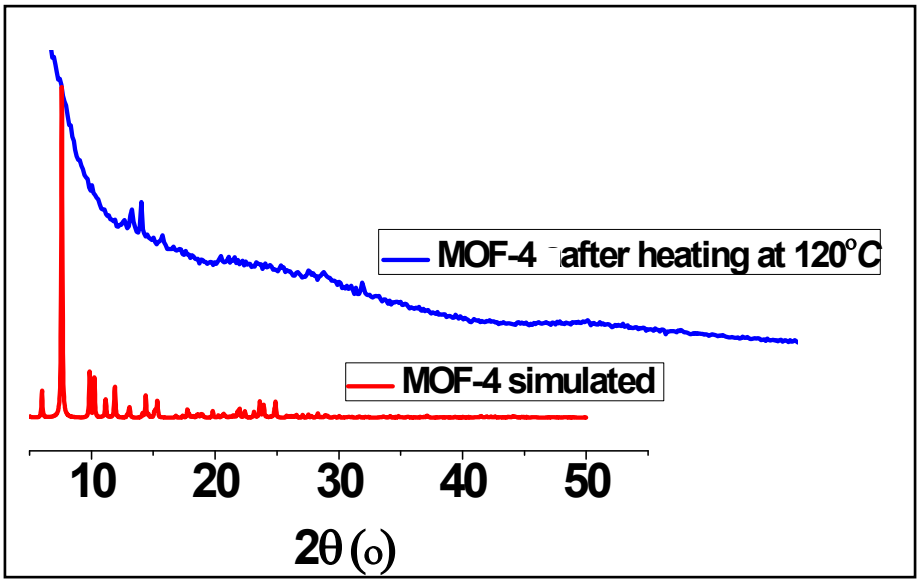

Figure S35: Comparison of PXRD patterns of MOF-**4** after heat treatment.